 CMES, vol.54, no.2, pp.201-221, 2009

An Iterative Time-Domain Algorithm for Acoustic-Elastodynamic Coupled Analysis Considering Meshless Local Petrov-Galerkin Formulations

Delfim Soares Jr.[1]

Abstract: In this work, meshless methods based on the local Petrov-Galerkin approach are employed for the time-domain analysis of interacting fluid and solid systems. For the spatial discretization of the acoustic fluid and elastodynamic solid sub-domains involved in the coupled analyses, MLPG formulations adopting Gaussian weight functions as test functions are considered, as well as the moving least square method is used to approximate the incognita fields. For time discretization, the Houbolt's method is adopted. The fluid-solid coupled analysis is accomplished by an iterative algorithm. In this iterative approach, each sub-domain of the global model is analysed independently (as an uncoupled model) and a successive renewal of the variables at the common interfaces is performed, until convergence is achieved. At the end of the paper, numerical applications illustrate the accuracy and potentialities of the proposed techniques.

Keywords: Meshless Local Petrov-Galerkin, Moving Least Squares, Acoustic Fluids, Elastodynamic Solids, Time-Domain Analysis, Iterative Coupling.

1 Introduction

The investigation of interacting fluid and solid systems (e.g., fluids, such as air, water, lubricants, blood etc., coupled with structural elements, such as buildings, dams, offshore structures, mechanical components, pressure vessels, live organs etc.) is a research field of particular importance in engineering and science. In many cases, this interaction is quite expressive and must not be neglected, otherwise the related analyses may only represent a very crude approximation of the real model (this is particularly true in the case of a heavy fluid, such as water, interacting with a rather light solid, such as a membrane type structure). Up to now, although a considerable amount of publications is available concerning the numerical

[1] Structural Engineering Department, Federal University of Juiz de Fora, Cidade Universitária, CEP 36036-330, Juiz de Fora, MG, Brazil. Tel: +55 32 2102-3468; E-mail: delfim.soares@ufjf.edu.br

modelling of fluid-solid coupled systems (see, for instance, Belytschko and Geers, 1977; Mathews, 1986; von Estorff and Antes, 1991; Maman and Farhat, 1995; Farhat *et al*., 1998; Lie *et al*., 2001; Park *et al*., 2001; Czygan and von Estorff, 2002; Lombard and Piraux, 2004; Soares *et al*., 2005, 2007, 2010a; etc.) – several of them even considering the coupling of different numerical procedures – few publications concentrate on the topic when meshless techniques are focused; and, as far as the author is concerned, there are no publications on the matter considering meshless local Petrov-Galerkin (MLPG) formulations (for some key references concerning the MLPG, the reader is referred to Atluri and Zhu, 1998; Atluri and Shen, 2002a-b; Atluri, 2004; etc.; for some interesting applications of the MLPG to solid and fluid analyses, the reader is referred to Han et al., 2005, 2006; Ma, 2005; Mohammadi, 2008; Long et al., 2008; etc.).

In the beginning of the decade, Beckert and Wendland (2001) presented a multivariate interpolation scheme for coupling fluid (CFD) and structural models (FE) in three-dimensional space using radial basis functions, applying the procedure to analyse typical static aeroelastic problems. Latter on, Ahrem *et al.* (2006) presented a meshless spatial coupling scheme for large-scale fluid-structure interaction problems, allowing the coupling of arbitrary meshes on fluid and structure sides. The scheme was based upon a multivariate scattered data interpolation approach, radial basis functions and partition of unity methods. Some years latter, Rendall and Allen (2008) presented a multivariate interpolation scheme, using radial basis functions, which removed all volume/structural mesh and flow-solver type dependence, allowing all operations to be performed on totally arbitrary point clouds. Recently, this procedure has been improved by the authors, taking into account localized implementation (Rendall and Allen, 2009).

In this work, the coupling of acoustic fluids and elastodynamic solids modelled by MLPG formulations is discussed. In order to deal with the coupled analysis in focus, a time-domain iterative coupling algorithm is adopted, allowing each fluid and solid sub-domain of the global model to be analysed independently. This is a quite attractive approach for fluid-solid coupled analyses, since it avoids the computation (as well as the solution) of the rather big and complex coupled system of equations that is related to these kind of models. This alternative iterative coupling methodology was first developed, to analyse two-dimensional fluid-solid coupled systems, taking into account finite element – boundary element coupled formulations (Soares *et al*., 2005). Later on, it was extended to analyse more generic fluid-solid coupled models (Soares and Mansur, 2006; Warszawski *et al*., 2008; Soares, 2008, 2009).

The present paper is organized as follows: first (section 2), the governing equations for the fluid and solid sub-domains are presented, as well as their coupling

equations. In the sequence, the spatial and temporal discretizations for the different sub-domains are briefly described (section 3) and the iterative coupling algorithm is discussed (section 4). At the end of the paper (section 5), numerical results are presented, illustrating the accuracy and potentialities of the proposed methodology.

2 Governing Equations

In the present section, acoustic and elastic wave equations are briefly presented. These wave propagation models are used to model the fluid and solid sub-domains of the global problem, respectively. At the end of the section, basic equations concerning the coupling of acoustic and elastic sub-domains are described.

2.1 Fluid sub-domains

If the influence of gravity on the dynamic behavior of the fluid is neglected, the hydrodynamic equilibrium and continuity fluid equations lead to the so-called scalar wave equation:

$$(\kappa p_{,i})_{,i} - \rho \ddot{p} + S = 0 \tag{1}$$

which describes the irrotational small-amplitude motions of the fluid particles. In equation (1), $p(X,t)$ stands for hydrodynamic pressure distribution and $S(X,t)$ for body source terms. Inferior commas (indicial notation is adopted) and over dots indicate partial space ($p_{,i} = \partial p/\partial x_i$) and time ($\dot{p} = \partial p/\partial t$) derivatives, respectively. $\rho(X)$ stands for the mass density and $\kappa(X)$ is the bulk modulus of the medium. In homogeneous media, ρ and κ are constant and the classical wave equation can be written as:

$$p_{,ii} - (1/c^2)\ddot{p} + s = 0 \tag{2}$$

where $c = \sqrt{\kappa/\rho}$ is the wave propagation velocity. The boundary and initial conditions of the problem are given by:

(i) Boundary conditions ($t > 0$, $X \in \Gamma$ where $\Gamma = \Gamma_1 \cup \Gamma_2$)

$$p(X,t) = \bar{p}(X,t) \text{ for } X \in \Gamma_1 \tag{3a}$$

$$q(X,t) = p_{,j}(X,t)n_j(X) = \bar{q}(X,t) \text{ for } X \in \Gamma_2 \tag{3b}$$

(ii) Initial conditions ($t = 0$, $X \in \Gamma \cup \Omega$):

$$p_i(X,0) = \bar{p}_{i0}(X) \tag{4a}$$

$$\dot{p}(X,0) = \dot{\bar{p}}_0(X) \tag{4b}$$

where the prescribed values are indicated by over bars and q represents the flux along the boundary whose unit outward normal vector components are represented by n_j. The boundary of the model is denoted by $\Gamma(\Gamma_1 \cup \Gamma_2 = \Gamma$ and $\Gamma_1 \cap \Gamma_2 = 0)$ and the domain by Ω.

2.2 Solid sub-domains

The elastic wave equation for homogenous media is given by:

$$(c_d^2 - c_s^2)u_{j,ji} + c_s^2 u_{i,jj} - \ddot{u}_i + b_i = 0 \tag{5}$$

where u_i and b_i stand for the displacement and the body force distribution components, respectively. The notation for time and space derivatives employed in equation (1) is once again adopted. In equation (5), c_d is the dilatational wave velocity and c_s is the shear wave velocity, they are given by: $c_d^2 = (\lambda + 2\mu)/\rho$ and $c_s^2 = \mu/\rho$, where ρ is the mass density and λ and μ are the Lamé's constants of the medium. Equation (5) can be obtained from the combination of the following basic mechanical equations (proper to model heterogeneous media):

$$\sigma_{ij,j} - \rho\ddot{u}_i + \rho b_i = 0 \tag{6a}$$

$$\sigma_{ij} = \lambda\,\delta_{ij}\varepsilon_{kk} + 2\mu\varepsilon_{ij} \tag{6b}$$

$$\varepsilon_{ij} = \tfrac{1}{2}(u_{i,j} + u_{j,i}) \tag{6c}$$

where σ_{ij} and ε_{ij} are, respectively, stress and strain tensor components and δ_{ij} is the Kronecker delta (δ_{ij} = 1, for $i = j$ and δ_{ij} = 0, for $i \neq j$). Equation (6a) is the momentum equilibrium equation; equation (6b) represents the constitutive law of the model and equation (6c) stands for kinematical relations. The boundary and initial conditions of the elastodynamic problem are given by:

(i) Boundary conditions ($t > 0, X \in \Gamma$ where $\Gamma = \Gamma_1 \cup \Gamma_2$)

$$u_i(X,t) = \bar{u}_i(X,t) \text{ for } X \in \Gamma_1 \tag{7a}$$

$$\tau_i(X,t) = \sigma_{ij}(X,t)n_j(X) = \bar{\tau}_i(X,t) \text{ for } X \in \Gamma_2 \tag{7b}$$

(ii) Initial conditions (t = 0, $X \in \Gamma \cup \Omega$)

$$u_i(X,0) = \bar{u}_{i0}(X) \tag{8a}$$

$$\dot{u}_i(X,0) = \dot{\bar{u}}_{i0}(X) \tag{8b}$$

where, once again, the prescribed values are indicated by over bars and τ_i denotes the traction vector along the boundary (n_j, as indicated previously, stands for the components of the unit outward normal vector).

2.3 Fluid-solid interacting interfaces

On the fluid-solid interface boundaries, the elastic sub-domain normal (normal to the interface) accelerations ($\ddot{u}_n$) are related to the acoustic sub-domain fluxes (q), and the acoustic sub-domain hydrodynamic pressures (p) are related to the elastic sub-domain normal tractions (τ_n). These relations are expressed by the following equations:

$$\ddot{u}_n - (1/\rho)q = 0 \tag{9a}$$

$$\tau_n + p = 0 \tag{9b}$$

where in equations (9) the sign of the different sub-domain outward normal directions is taken into account (outward normal vectors on the same interface point are opposite for each sub-domain). In equation (9a), ρ is the mass density of the interacting fluid sub-domain.

3 Numerical discretization

In this section, the numerical discretization of the fluid and solid sub-domains by meshless local Petrov-Galerkin formulations is briefly discussed. First, in subsection 3.1, the moving least square (MLS) approximation is described and, next (sub-sections 3.2 and 3.3), the local weak-forms for the fluid and solid sub-domains, as well as their spatial discretizations taking into account MLS approximations, are discussed. In sub-section 3.4, time-marching procedures based on the Houbolt's method are presented, allowing the time-domain solution of the matricial systems of equations that arise.

3.1 Moving least square approximation

In general, a meshless method uses a local approximation to represent the trial function in terms of nodal unknowns which are either the nodal values of real field variables or fictitious nodal unknowns at some randomly located nodes. The moving least squares approximation may be considered as one of such schemes, and it is used here.

Consider a sub-domain Ω_x, the neighbourhood of a point X and denoted as the domain of definition of the MLS approximation for the trial function at X, which is located in the problem domain Ω (see Fig.1). Also consider a generic field ϕ, which represents the hydrodynamic pressure field p, in case of fluid sub-domains analyses, or the displacement field u_i, in case of solid sub-domains modelling. To approximate the distribution of function ϕ in Ω_x, over a number of randomly located nodes, the MLS approximation of ϕ can be defined by (Atluri and Shen,

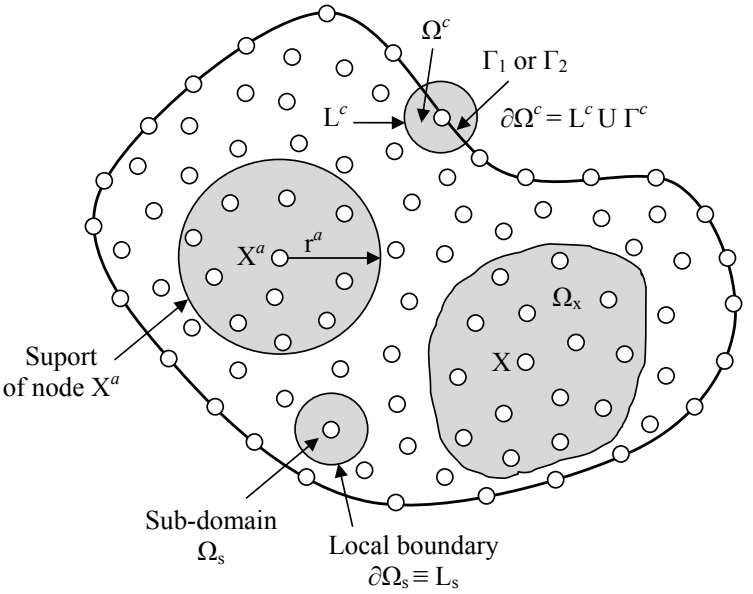

Figure 1: Local boundaries, sub-domains and domain of definition of the MLS approximation for the trial function at node X.

2002a; Atluri, 2004):

$$\phi(X,t) \approx \Pi^T(X)\hat{\Phi}(t) = \sum_{a=1}^{N} \eta^a(X)\hat{\phi}^a(t) \tag{10}$$

where $\hat{\phi}$ is the fictitious nodal value of ϕ and N is the number of points in the sub-domain Ω_x. The shape matrix $\Pi^T(X) = [\eta^1(X), \eta^2(X), \ldots, \eta^N(X)]$ is computed by:

$$\Pi^T(X) = \mathbf{p}^T(X)\mathbf{A}^{-1}(X)\mathbf{B}(X) \tag{11}$$

where

$$\mathbf{A}(X) = \sum_{a=1}^{N} w^a(X)\mathbf{p}(X^a)\mathbf{p}^T(X^a) \tag{12a}$$

$$\mathbf{B}(X) = [w^1(X)\mathbf{p}(X^1),\ w^2(X)\mathbf{p}(X^2),\ ....,\ w^N(X)\mathbf{p}(X^N)] \tag{12b}$$

and $\mathbf{p}^T(X) = [p_1(X),\ p_2(X),\ \ldots,\ p_m(X)]$ is a complete monomial basis of order m. $w^a(X)$ is the weight function associated with node a. The Gaussian weight function

is adopted here, and it is given by:

$$w^a(X) = \frac{\exp[-(d_a/c_a)^{2k}] - \exp[-(r_a/c_a)^{2k}]}{1-\exp[-(r_a/c_a)^{2k}]}(1-H[d_a-r_a]) \tag{13}$$

where $d_a = ||X - X^a||$ is the distance between the sampling point X and node X^a, c_a is a constant controlling the shape of the weight function and r_a is the radius of the circular support of the weight function. The Heaviside unit step function is defined as $H[z] = 1$ for $z > 0$ and $H[z] = 0$ for $z \leq 0$. The size of the weight function support should be large enough to have a sufficient number of nodes covered in the domain of definition to ensure the regularity of matrix $\mathbf{A}$.

3.2 Fluid discretization

Instead of writing the global weak-form for the governing equations described in section 2, the MLPG method constructs a weak-form over local fictitious sub-domains, such as Ω_s, which is a small region taken for each node inside the global domain (see Fig.1). The local sub-domains overlap each other, and cover the whole global domain Ω. The geometrical shape and size of local sub-domains can be arbitrary. In the present work, the local sub-domains are taken to be of circular shape. The local weak-form of the governing equations described in sub-section 2.1 can be written as:

$$\int_{\partial\Omega_s} \varphi\kappa q d\Gamma - \int_{\Omega_s} \varphi_{,i}\kappa p_{,i} d\Omega + \int_{\Omega_s} \varphi(S-\rho\ddot{p}) d\Omega + \beta \int_{\Gamma_{s1}} \varphi(p-\bar{p}) d\Gamma = 0 \tag{14}$$

where φ is a test function and β is a penalty parameter, which is introduced here in order to impose essential prescribed boundary conditions in an integral form. In equation (14), $\partial\Omega_s$ is the boundary of the local sub-domain, which consists of three parts, in general: $\partial\Omega_s = L_s \cup \Gamma_{s1} \cup \Gamma_{s2}$. Here, L_s is the local boundary that is totally inside the global domain, Γ_{s2} is the part of the local boundary which coincides with the global natural boundary, i.e., $\Gamma_{s2} = \partial\Omega_s \cap \Gamma_2$, and similarly Γ_{s1} is the part of the local boundary that coincides with the global essential boundary, i.e., $\Gamma_{s1} = \partial\Omega_s \cap \Gamma_1$ (see Fig.1).

Equation (14) can be rewritten by taking into account approximation (10) and by defining the local integral sub-domain as the circle Ω^c, centred at node $X^c$and described by radius r_c. The expression that arises, considering the test functions spec-

ified as $\varphi = w^c$ (Gaussian weight function), is given by:

$$\sum_{a=1}^{N}\left[\left(\int_{\Omega^c} w^c \rho \eta^a d\Omega\right)\ddot{\hat{p}}^a - \left(\beta\int_{\Gamma_1^c} w^c \eta^a d\Gamma + \int_{\Gamma_1^c} w^c \kappa n_i \eta^a_{,i} d\Gamma - \int_{\Omega^c} w^c_{,i}\kappa\eta^a_{,i} d\Omega\right)\hat{p}^a\right] = \\ = \int_{\Gamma_2^c} w^c \kappa \bar{q} d\Gamma + \int_{\Omega^c} w^c S d\Omega - \beta\int_{\Gamma_1^c} w^c \bar{p} d\Gamma \quad (15)$$

By collecting all nodal unknown fictitious values $\hat{p}^a(t)$ into vector $\hat{\mathbf{P}}$, the system of the discretized equations (15) can be rewritten into matrix form, as follows:

$$\mathbf{M}\ddot{\hat{\mathbf{P}}} + \mathbf{K}\hat{\mathbf{P}} = \mathbf{F} \quad (16)$$

where $\mathbf{M}$ is the matrix evaluated taking into account the first integral term on the l.h.s. of equations (15); $\mathbf{K}$ is the matrix computed considering the second terms on the l.h.s. of equations (15); and $\mathbf{F}$ is the vector evaluated considering the terms on the r.h.s. of equations (15). Once the second order ordinary differential matrix equation (16) is established, its solution in the time-domain is discussed in sub-section 3.4, taking into account finite difference procedures.

3.3 Solid discretization

The local weak-form of the governing equations described in sub-section 2.2 is written as:

$$\int_{\partial\Omega_s} \varphi_{ik}\sigma_{ij}n_j d\Gamma - \int_{\Omega_s} \varphi_{ik,j}\sigma_{ij} d\Omega + \int_{\Omega_s} \varphi_{ik}(\rho b_i - \rho\ddot{u}_i) d\Omega + \beta\int_{\Gamma_{s1}} \varphi_{ik}(u_i - \bar{u}_i) d\Gamma = 0 \quad (17)$$

where, once again, φ_{ik} is a test function and β is a penalty parameter.

Analogously to equation (14), equation (17) can be rewritten taking into account approximation (10) and specifying the local integral sub-domain as the circle Ω^c centred at node X^c. Considering the test functions specified as $\varphi_{ik} = \delta_{ik}w^c$ (Gaussian weight function) and adopting Voigt notation, the expression that arises is given by:

$$\sum_{a=1}^{N}\left[\left(\int_{\Omega^c} w^c \rho \eta^a d\Omega\right)\ddot{\hat{\mathbf{u}}}^a - \left(\beta\int_{\Gamma_1^c} w^c \eta^a d\Gamma + \int_{\Gamma_1^c} w^c \mathbf{N}\mathbf{D}\mathbf{B}^a d\Gamma - \int_{\Omega^c} \mathbf{W}^c\mathbf{D}\mathbf{B}^a d\Omega\right)\hat{\mathbf{u}}^a\right] = \\ = \int_{\Gamma_2^c} w^c \bar{\tau} d\Gamma + \int_{\Omega^c} w^c \rho \mathbf{b} d\Omega - \beta\int_{\Gamma_1^c} w^c \bar{\mathbf{u}} d\Gamma \quad (18)$$

where $\mathbf{N}$ is the normal matrix, $\mathbf{D}$ is the constitutive matrix, $\mathbf{B}^a$ is the strain matrix (defined by a combination of the spatial derivatives of the interpolation functions η^a) and $\mathbf{W}^c$ is defined by a combination of the spatial derivatives of the weight functions w^c (analogously to the definition of the transpose of the strain matrix).

By collecting all nodal unknown fictitious displacements $\hat{u}^a(t)$ into vector $\hat{\mathbf{U}}$, the system of the discretized equations (18) can be rewritten into matrix form, as follows:

$$\mathbf{M}\ddot{\hat{\mathbf{U}}} + \mathbf{K}\hat{\mathbf{U}} = \mathbf{F} \tag{19}$$

where the definitions of the matrices and vectors specified in equation (19) are analogous to those of equation (16).

3.4 Temporal discretization

The Houbolt's method is considered here to solve the systems of second order ordinary differential equations (16) and (19) in the time-domain (Houbolt, 1950). It is important to observe that the Houbolt's method provides high-frequency dissipation, eliminating the contribution of spurious modes, which is of great importance considering MLPG formulations, in order to avoid unstable results. In the Houbolt's method, the following finite difference expression is considered in order to approximate $\ddot{\hat{\Phi}}$ (once again, $\hat{\Phi}$ is here employed to generically represent $\hat{\mathbf{P}}$ or $\hat{\mathbf{U}}$) at time t^{n+1}:

$$\ddot{\hat{\Phi}}^{n+1} = (2\hat{\Phi}^{n+1} - 5\hat{\Phi}^n + 4\hat{\Phi}^{n-1} - \hat{\Phi}^{n-2})/\Delta t^2 \tag{20}$$

where Δt is a selected time-step.

After introducing relation (20) into the systems of equations (16) or (19), the following system of equations arises, which allows the computation of the fictitious nodal values $\hat{\phi}$ at each time-step:

$$\bar{\mathbf{A}}\hat{\Phi}^{n+1} = \bar{\mathbf{B}} \tag{21}$$

where $\bar{\mathbf{A}}$ and $\bar{\mathbf{B}}$ are the Houlbot's effective matrix and vector, respectively, given by:

$$\bar{\mathbf{A}} = (2/\Delta t^2)\mathbf{M} + \mathbf{K} \tag{22a}$$

$$\bar{\mathbf{B}} = \mathbf{F}^{n+1} + (1/\Delta t^2)\mathbf{M}(5\hat{\Phi}^n - 4\hat{\Phi}^{n-1} + \hat{\Phi}^{n-2}) \tag{22b}$$

4 Fluid-solid coupling

In order to perform the coupling of the fluid/solid sub-domains, each sub-domain is analysed independently here (i.e., as an uncoupled model) and a successive renewal of the variables at the common interfaces is performed through an iterative procedure until convergence is achieved. As previously reported (Soares *et al.*, 2005), several advantages arise from iterative coupling approaches considering fluid-solid interacting models, as for instance: (i) simpler, smaller and better-conditioned systems of equations are obtained, leading to more efficient numerical analyses; (ii) only interface routines are required when one wishes to use existing codes to build coupling algorithms; (iii) nonlinearities can be taken into account in the same iteration loop needed for the coupling and, as a consequence, consideration of nonlinear models (not focused on this work) does not introduce a relevant CPU time increase; etc.

In the next sub-section, the calculus of the coupling matrices and forces is described, taking into account MLPG formulations. In the sequence, the fluid-solid iterative coupling algorithm is discussed in detail.

4.1 Coupling matrices and forces

In the iterative coupling approach being considered, natural boundary conditions are prescribed, at the common interfaces, for each sub-domain. The accelerations evaluated at the solid sub-domains are used to obtain the fluxes (prescribed interface boundary condition) for the fluid sub-domains (equation (9a)) and the pressures evaluated at the fluid sub-domains are used to obtain the tractions (prescribed interface boundary condition) for the solid sub-domains (equation (9b)).

Taking into account equation (9a), the coupling forces acting on a fluid sub-domain, due to an interacting solid sub-domain, can be written locally (i.e., at the local integral circle sub-domain centred at the interface node X^i) as:

$$\mathbf{f}_{\ddot{u}} = \int_{\Gamma_2^i} w^i \kappa \bar{q} d\Gamma = \int_{\Gamma_2^i} w^i \kappa \rho \mathbf{n}^T \ddot{\mathbf{u}} d\Gamma = \sum_{a=1}^{N} \left(\int_{\Gamma_2^i} w^i \kappa \rho \mathbf{n}^T \eta^a d\Gamma \right) \ddot{\mathbf{u}}^a \tag{23}$$

where $\mathbf{n} = [n_1, n_2]^T$ is the solid sub-domain unit outward normal vector. By collecting all nodal values into global vectors, equation (23) can be rewritten into matrix form, as follows:

$$\mathbf{F}_{\ddot{u}} = \mathbf{Q}_{\ddot{u}} \ddot{\hat{\mathbf{U}}} \tag{24}$$

where $\mathbf{Q}_{\ddot{u}}$ is the fluid-solid coupling matrix.

Taking into account equation (9b), the coupling forces acting on a solid sub-domain, due to an interacting fluid sub-domain, can be written locally as:

$$\mathbf{f}_p = \int_{\Gamma_2^i} w^i \bar{\tau} d\Gamma = \int_{\Gamma_2^i} w^i \mathbf{n}\, p d\Gamma = \sum_{a=1}^{N} \left(\int_{\Gamma_2^i} w^i \mathbf{n} \eta^a d\Gamma \right) \hat{p}^a \tag{25}$$

where $\mathbf{n}$ is the fluid sub-domain unit outward normal vector. Analogously to equation (23), equation (25) can be rewritten into matrix form, as follows:

$$\mathbf{F}_p = \mathbf{Q}_p \hat{\mathbf{P}} \tag{26}$$

where $\mathbf{Q}_p$ is the solid-fluid coupling matrix.

Taking into account the coupling forces $\mathbf{F}_{\ddot{u}}$ and $\mathbf{F}_p$, the fluid and solid discrete governing equations (16) and (19) can be rewritten together as:

$$\mathbf{M}\ddot{\hat{\mathbf{P}}} + \mathbf{K}\hat{\mathbf{P}} = \mathbf{F} + \mathbf{F}_{\ddot{u}} \tag{27a}$$

$$\mathbf{M}\ddot{\hat{\mathbf{U}}} + \mathbf{K}\hat{\mathbf{U}} = \mathbf{F} + \mathbf{F}_p \tag{27b}$$

where in the coupled equations (27) the effects of the interacting sub-domains are being considered.

4.2 Iterative coupling algorithm

Initially, in the fluid-solid iterative coupling algorithm, the solid sub-domain is analysed and the solid displacements and accelerations are evaluated taking into account equations (27b) and (20), respectively (i.e., ${}^{(k+\alpha)}\hat{\mathbf{U}}^{n+1}$ and ${}^{(k+\alpha)}\ddot{\hat{\mathbf{U}}}^{n+1}$ are computed, where left superscripts stand for iterative steps. For the first iterative step of each time step, ${}^{(0)}\mathbf{F}_p^{n+1} = \mathbf{Q}_p \hat{\mathbf{P}}^n$ is assumed). In the sequence, a relaxation parameter α ($0 < \alpha \leq 1$) is introduced in order to ensure and/or to speed up convergence, such that:

$${}^{(k+1)}\ddot{\hat{\mathbf{U}}}^{n+1} = (\alpha)\,{}^{(k+\alpha)}\ddot{\hat{\mathbf{U}}}^{n+1} + (1-\alpha)\,{}^{(k)}\ddot{\hat{\mathbf{U}}}^{n+1} \tag{28}$$

Once ${}^{(k+1)}\ddot{\hat{\mathbf{U}}}^{n+1}$ is calculated, the fluid coupling force ${}^{(k+1)}\mathbf{F}_{\ddot{u}}^{n+1}$ is evaluated according to equation (24). Taking into account the effects of force ${}^{(k+1)}\mathbf{F}_{\ddot{u}}^{n+1}$, the fluid sub-domain is analysed, as described by equation (27a), and the hydrodynamic pressures ${}^{(k+1)}\hat{\mathbf{P}}^{n+1}$ are computed. Once ${}^{(k+1)}\hat{\mathbf{P}}^{n+1}$ is computed, the solid coupling force ${}^{(k+1)}\mathbf{F}_p^{n+1}$ is evaluated according to equation (26) and the solid sub-domain is once again analysed considering the effects of ${}^{(k+1)}\mathbf{F}_p^{n+1}$, reinitiating the iterative cycle.

The following convergence criterion may be considered for the iterative procedure:

$$||^{(k+1)}\hat{\Phi}^{n+1} - {}^{(k)}\hat{\Phi}^{n+1}||/||^{(k)}\hat{\Phi}^{n+1}|| \leq \xi \tag{29}$$

where ξ stands for a pre-selected tolerance error and $\hat{\Phi}$ represents the displacements at the solid sub-domains, the hydrodynamic pressures at the fluid sub-domains, or both.

5 Numerical aspects and applications

Two numerical applications are considered here, illustrating the discussed methodologies. In the first application, a fluid-solid column is analysed and the obtained results are compared to analytical answers. In the second application, a dam-reservoir system is studied and the computed responses are compared to those provided by a FEM-BEM coupled analysis.

In the present work, the radii of the influence domain and of the local sub-domain are set to $\theta_x d_i^3$ and $\theta_s d_i^1$, respectively; where d_i^3 and d_i^1 are the distances to the third and first nearest points from node i, respectively. In all the applications that follow, $\theta_x = 4.0$ and $\theta_s = 1.0$ are selected. Taking into account the number of terms in the definition of the basis vector $\mathbf{p}$, $m = 6$ is considered (quadratic basis). The $\mathbf{M}$ matrix is adopted diagonal (it is diagonalized by a row-sum technique), which allows a very efficient time-marching procedure, once the computational cost of the effective vector evaluation is considerably reduced (see equation (22b)). Regarding the iterative process, for all the applications that follow, a tight tolerance error of $\xi = 10^{-6}$ is adopted.

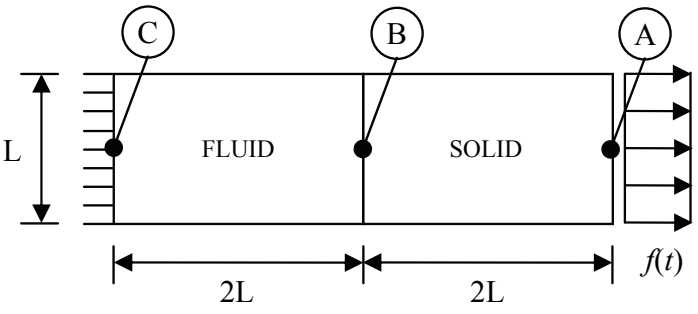

Figure 2: Sketch of the fluid-solid column.

5.1 Fluid-solid column

In this sub-section, a fluid-solid column is analysed (Soares *et al.*, 2007; Warszawski *et al.*, 2008). A sketch of the problem is depicted in Fig.2. The geometry of the model is defined by $L = 1.0m$ and the column is submitted to a time Heavisite force acting at one of its ends. The physical properties of the media are: (i) fluid sub-domain – $\kappa = 100N/m^2$ (bulk modulus) and $\rho = 1kg/m^3$ (density); (ii) solid sub-domain – $E = 100N/m^2$ (Young modulus), $\nu = 0$ (Poisson rate) and $\rho = 1kg/m^3$ (density). Two spatial-temporal discretizations are considered to analyse the model, namely: (i) discretization 1 – 153 nodes are employed to spatially discretize each sub-domain, in a regular equally spaced 9x17 (vertical and horizontal, respectively) distribution, and the time-step adopted is $\Delta t = 0.0025s$; (ii) discretization 2 – 561 nodes are employed to spatially discretize each sub-domain, in a regular equally spaced 17x33 (vertical and horizontal, respectively) distribution, and the time-step adopted is $\Delta t = 0.00125s$.

In Fig.3, displacement time-history results at points A and B of the solid sub-domain are plotted, considering discretizations 1 and 2. In Fig.4, analogous time-history results are depicted at points B and C, considering hydrodynamic pressures at the fluid sub-domain. Analytical time-histories (Miles, 1961) are also depicted in Figs. 3 and 4, highlighting the good accuracy of the numerical results.

Table 1: Average number of iterations per time-step considering different relaxation parameters for the fluid-solid column analyses

Relaxation Parameter	Discretization 1	Discretization 2
1.0	5.02	4.90
0.9	4.84	4.67
0.8	6.04	5.87
0.7	7.23	6.98
0.6	8.59	8.25
0.5	10.23	9.82

The oscillatory behaviour depicted in Fig.4 is typical for the present column analysis, even considering acoustic or elastodynamic uncoupled models analysed by different numerical procedures (e.g., finite elements, boundary elements etc.). In fact, the application in focus is a very important benchmark since the analytical answer is known and it represents a rather complex numerical computation (in spite of its geometrical and load simplicity) once there are successive reflections occurring at the model extremities and these multiple reflections can emphasize some numerical aspects, such as instabilities and excessive numerical damping.

(a)

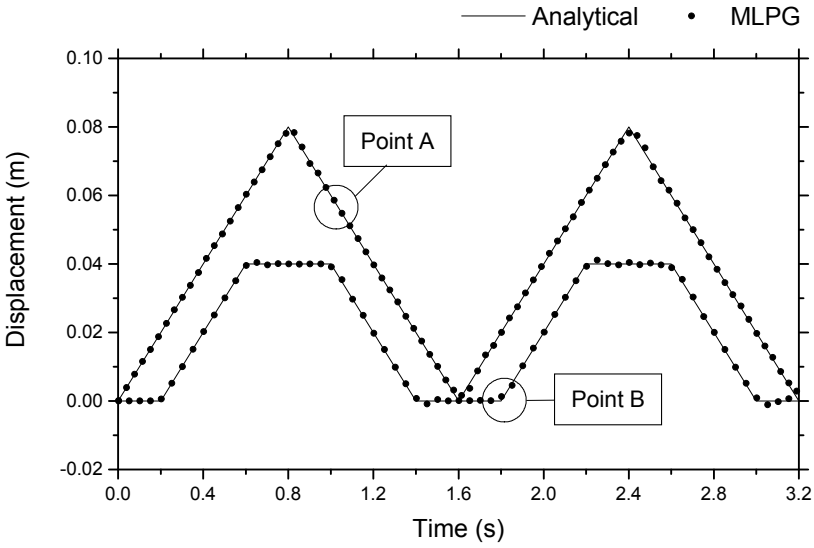

(b)

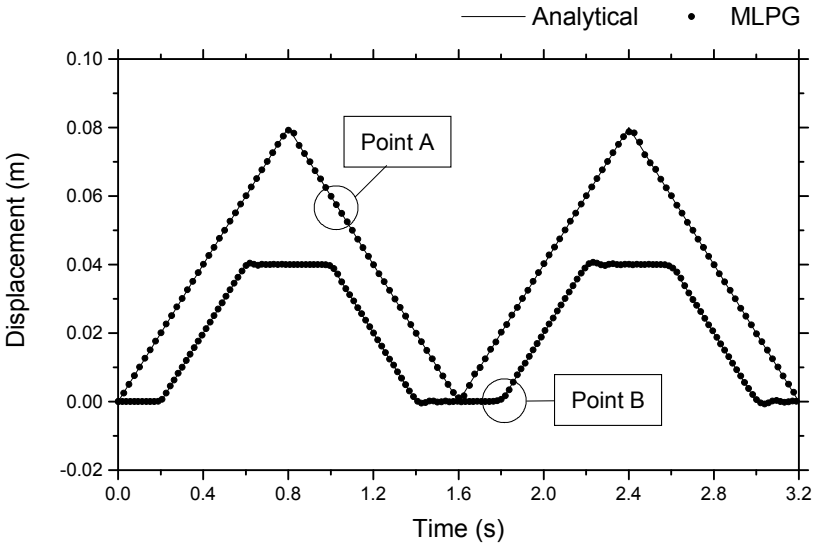

Figure 3: Time-history results for the horizontal displacements at points A and B: (a) discretization 1; (b) discretization 2.

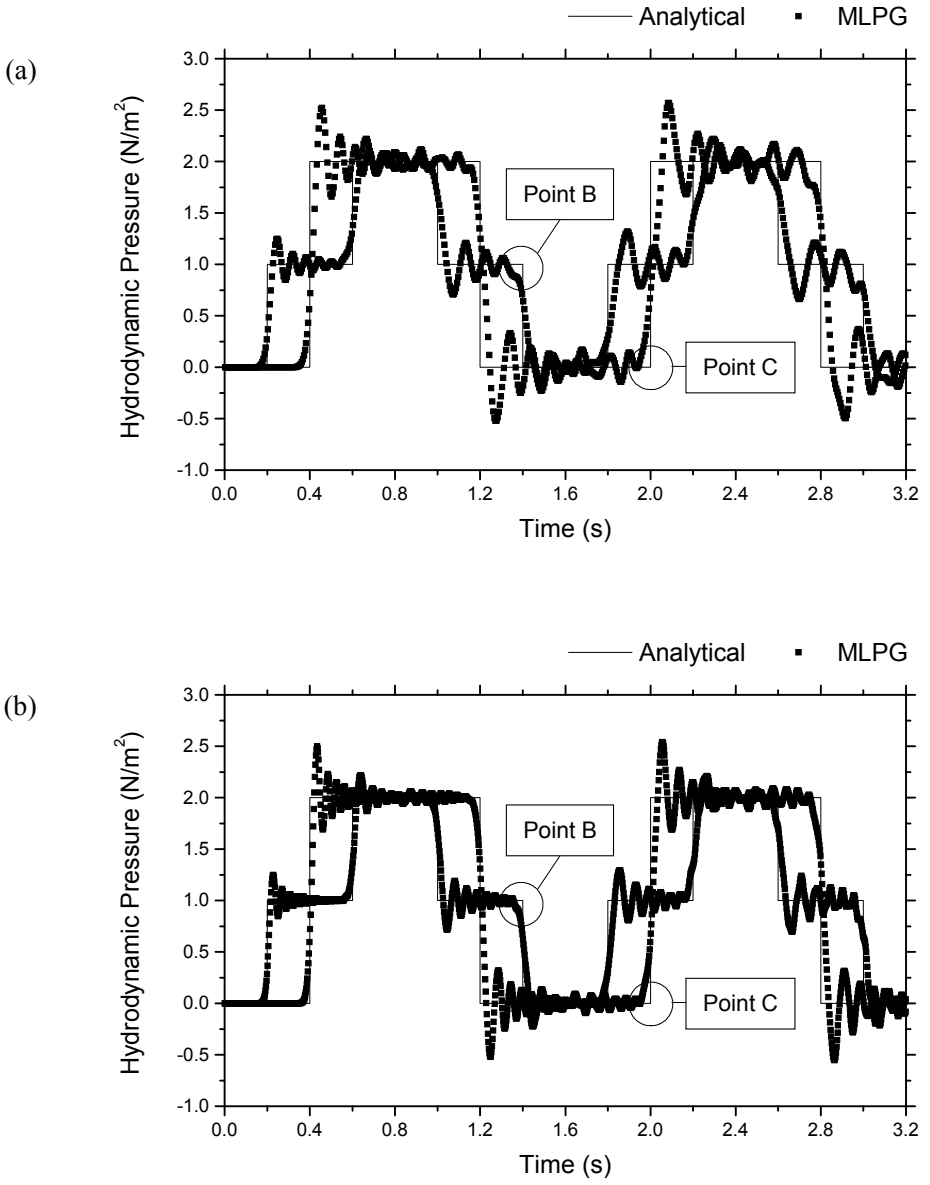

Figure 4: Time-history results for the hydrodynamic pressures at points B and C: (a) discretization 1; (b) discretization 2.

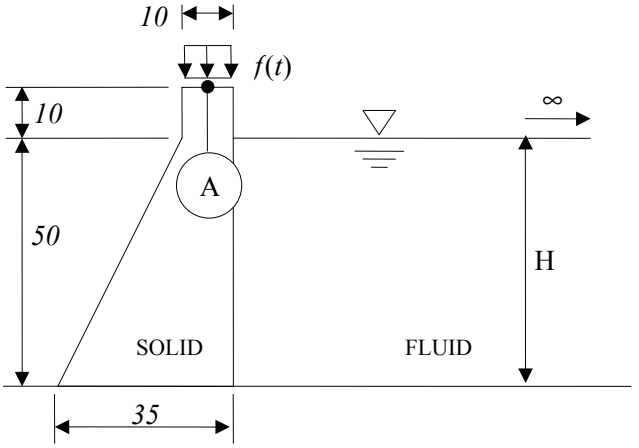

Figure 5: Sketch of the dam-reservoir system.

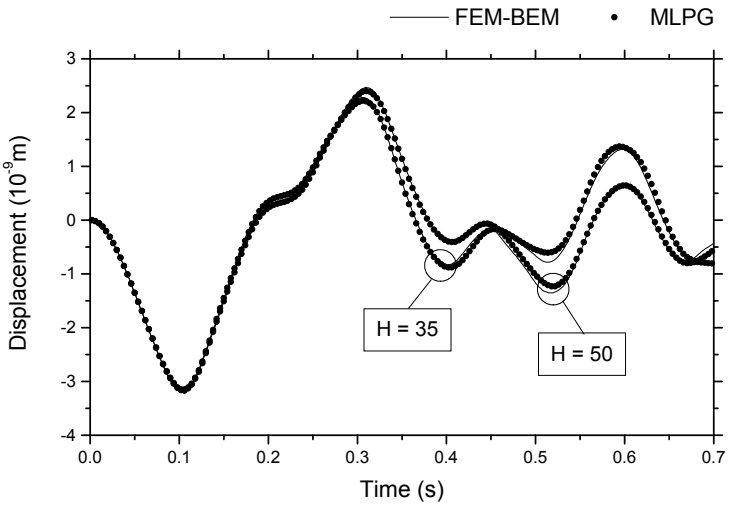

Figure 6: Time-history results for vertical displacements at point A considering H = 35m and H = 50m.

Table 2: Average number of iterations per time-step considering different relaxation parameters for the dam-reservoir system analyses

Relaxation Parameter	H=35	H=50
1.0	8.49	8.33
0.75	6.79	6.47
0.50	11.61	11.08
0.25	23.94	21.13

In Table 1, the average number of iterations per time step is presented, considering different relaxation parameter values. As one can observe, few iterations are necessary for the iterative algorithm to converge, once an appropriate relaxation parameter is selected (one should keep in mind that a tight tolerance error is being considered).

5.2 Dam-reservoir system

In this second example, a dam-reservoir system (von Estorff and Antes, 1991; Soares *et al*. 2005), as depicted in Fig. 5, is analysed. The structure is subjected to a sinusoidal distributed vertical load on its crest, acting with an angular frequency $w = 18$ *rad/s*. The material properties of the dam are: $E = 3.437 \cdot 10^9 N/m^2$, $\nu = 0.25$ and $\rho = 2000$ kg/m^3. The adjacent water is characterized by $c = 1436 m/s$ and $\rho = 1000$ kg/m^3 (water levels defined by H = 50 *m* and H = 35 *m* are considered). 113 nodes are employed to discretize the dam and the fluid is discretized by a regular equally spaced (horizontally sufficiently extended) distribution of nodes. Regarding temporal discretization, the time-step adopted for the analyses is $\Delta t = 0.002 s$.

Fig.6 depicts the vertical displacement time-histories at the dam crest (point A), taking into account the present MLPG coupled formulation and FEM-BEM coupled procedures (Soares *et al*. 2005). As one can observe, the time responses are quite similar considering these two different methodologies. In Table 2, once again the average number of iterations per time step is presented, considering different relaxation parameter values.

6 Conclusions

In the present work, numerical analyses of fluid-solid coupled problems, taking into account MLPG formulations, are presented for the first time. The coupling of interacting acoustic fluids and elastodynamic solids are carried out here by means of a time domain iterative algorithm. This numerical procedure not only is easy to implement (it only requires interface routines), but also it is very efficient, allowing

each sub-domain of the global model to be analysed independently. As a consequence, smaller, simpler and better conditioned systems of equations arise, which are easier and faster to be computed and solved.

The framework presented in this paper is also appropriate to analyse more complex physical models, as for instance, models governed by geometrical and material nonlinear formulations. In this case: (i) non-linear numerical analyses can be taken into account in the same iterative loop needed for the fluid-solid coupling; (ii) meshless techniques may be considered very appropriate, not only to evaluate the current state of stresses properly (Soares *et al*., 2009, 2010b), but also to avoid detrimental element distortions (usual in Lagrangian finite element approaches).

Acknowledgement: The financial support by CNPq (*Conselho Nacional de Desenvolvimento Científico e Tecnológico*) and FAPEMIG (*Fundação de Amparo à Pesquisa do Estado de Minas Gerais*) is greatly acknowledged.

References

Ahrem, R.; Beckert, A.; Wendland, H. (2006): A meshless spatial coupling scheme for large-scale fluid-structure-interaction problems, *CMES: Computer Modeling in Engineering & Sciences* vol.12, pp. 121-136.

Atluri, S.N. (2004): *The Meshless Method (MLPG) for Domain & BIE Discretizations*, Tech Science Press, Encino, CA.

Atluri, S.N.; Shen, S. (2002a): *The Meshless Local Petrov-Galerkin (MLPG) Method*, Tech Science Press, Encino, CA.

Atluri, S.N.; Shen, S.P. (2002b): The meshless local Petrov-Galerkin (MLPG) method: A simple & less-costly alternative to the finite element and boundary element methods, *CMES: Computer Modeling in Engineering and Sciences* vol.3, pp. 11-51.

Atluri, S.N.; Zhu, T. (1998): A New Meshless Local Petrov-Galerkin (MLPG) Approach in Computational Mechanics, *Computational Mechanics* vol.22, pp. 117-127.

Beckert, A.; Wendland, H. (2001): Multivariate interpolation for fluid-structure-interaction problems using radial basis functions, *Aerospace Science and Technology* vol.5, pp. 125-134.

Belytschko, T.; Geers, T.L. (eds.) (1977): *Computational methods for fluid-structure interaction problems*, AMD vol.26, American Society of Mechanical Engineers, New York.

Czygan, O.; von Estorff, O. (2002): Fluid-structure interaction by coupling BEM

and nonlinear FEM, *Engineering Analysis with Boundary Elements* vol.26, pp. 773-779.

Farhat, C.; Lesoinne, M.; LeTallec, P. (1998): Load and motion transfer algortihms for fluid/structure interaction problems with non-matching discrete interfaces: momentum and energy conservation, optimal discretization and application to aeroelasticity, *Computer Methods in Applied Mechanics and Engineering* vol.157, pp. 95-114.

Han, Z.D.; Liu, H.T.; Rajendran, A.M.; Atluri, S.N. (2006): The Applications of Meshless Local Petrov-Galerkin (MLPG) Approaches in High-Speed Impact, Penetration and Perforation Problems, *CMES: Computer Modeling in Engineering & Sciences* vol.14, pp. 119-128.

Han, Z.D.; Rajendran, A.M.; Atluri, S.N. (2005): Meshless Local Petrov-Galerkin (MLPG) Approaches for Solving Nonlinear Problems with Large Deformations and Rotations, *CMES: Computer Modeling in Engineering & Sciences* vol.10, pp. 1-12.

Houbolt, J.C. (1950): A recurrence matrix solution for the dynamic response of elastic aircraft, *Journal of the Aeronautical Sciences* vol.17, pp. 540-550.

Lie, S.T.; Yu, G.Y.; Zhao, Z. (2001): Coupling of BEM/FEM for time domain structural-acoustic interaction problems, *CMES: Computer Modeling in Engineering & Sciences* vol.2, pp. 171-180.

Lombard, B.; Piraux, J. (2004): Numerical treatment of two-dimensional interfaces for acoustic and elastic waves, *Journal of Computational Physics* vol.195, pp. 90-116.

Long, S.Y.; Liu, K.Y.; Li, G.Y. (2008): An Analysis for the Elasto-Plastic Fracture Problem by the Meshless Local Petrov-Galerkin Method, *CMES: Computer Modeling in Engineering & Sciences* vol.28, pp. 203-216.

Ma, Q.W. (2005): MLPG Method Based on Rankine Source Solution for Simulating Nonlinear Water Waves, *CMES: Computer Modeling in Engineering & Sciences* vol.9, pp. 193-210.

Maman, N.; Farhat, C. (1995): Matching fluid and structure meshes for aeroelastic computations: a parallel approach, *Computer & Structures* vol.54, pp. 779-785.

Mathews, I.C. (1986): Numerical techniques for three-dimensional steady-state fluid-structure interaction, *Journal of the Acoustical Society of America* vol.79, pp. 1317-1325.

Miles, J.W. (1961): *Modern Mathematics for the Engineer* (Beckenbach, E.F., ed.), MacGraw-Hill, London.

Mohammadi, M.H. (2008): Stabilized Meshless Local Petrov-Galerkin (MLPG)

Method for Incompressible Viscous Fluid Flows, *CMES: Computer Modeling in Engineering & Sciences* vol.29, pp. 75-94.

Park, K.C., Felippa, C.A., Ohayon, R. (2001): Partioned formulation of internal fluid-structure interaction problems via localized Lagrange multipliers, *Computer Methods in Applied Mechanics and Engineering* vol.190, pp. 2989-3007.

Rendall, T.C.S.; Allen, C.B. (2008): Unified fluid-structure interpolation and mesh motion using radial basis function, *International Journal for Numerical Methods in Engineering* vol.74, pp. 1519-1559.

Rendall, T.C.S., Allen, C.B. (2009): Improved radial basis function fluid-structure coupling via efficient localized implementation, *International Journal for Numerical Methods in Engineering* vol.78, pp. 1188-1208.

Soares, D. (2008): Numerical modelling of acoustic-elastodynamic coupled problems by stabilized boundary element techniques, *Computational Mechanics* vol.42, pp. 787-802.

Soares, D. (2009): Fluid-structure interaction analysis by optimised boundary element – finite element coupling procedures, *Journal of Sound and Vibration* vol.322, pp. 184-195.

Soares, D.; Mansur, W.J. (2005): An efficient time-domain BEM/FEM coupling for acoustic-elastodynamic interaction problems, *CMES: Computer Modeling in Engineering & Sciences* vol.8, pp. 153-164.

Soares, D.; Mansur, W.J. (2006): Dynamic analysis of fluid–soil–structure interaction problems by the boundary element method, *Journal of Computational Physics* vol.219, pp. 498-512.

Soares, D.; Mansur, W.J.; Lima, D.L. (2007): An explicit multi-level time-step algorithm to model the propagation of interacting acoustic-elastic waves using finite element / finite difference coupled procedures, *CMES: Computer Modeling in Engineering & Sciences* vol.17, pp. 19-34.

Soares, D.; Rodrigues, G.G.; Gonçalves, K.A. (2010a): An efficient multi-time-step implicit-explicit method to analyze solid-fluid coupled systems discretized by unconditionally stable time-domain finite element procedures, *Computers & Structures* vol.88, pp. 387-394.

Soares, D.; Sladek, J.; Sladek, V. (2009): Dynamic analysis by meshless local Petrov-Galerkin formulations considering a time-marching scheme based on implicit Green's functions, *CMES: Computer Modeling in Engineering & Sciences* vol.50, pp. 115-140.

Soares, D.; Sladek, J.; Sladek, V. (2010b): Nonlinear dynamic analyses by meshless local Petrov-Galerkin formulations, *International Journal for Numerical Meth-*

ods in Engineering vol.81, pp. 1687-1699.

Soares, D.; von Estorff, O.; Mansur, W.J. (2005): Efficient nonlinear solid-fluid interaction analysis by an iterative BEM/FEM coupling, *International Journal for Numerical Methods in Engineering* vol.64, pp. 1416-1431.

von Estorff, O.; Antes, H. (1991): On FEM-BEM coupling for fluid-structure interaction analysis in the time domain, *International Journal for Numerical Methods in Engineering* vol.31, pp. 1151-1168.

Warszawski, A.; Soares, D.; Mansur, W.J. (2008): A FEM-BEM coupling procedure to model the propagation of interacting acoustic-acoustic / acoustic-elastic waves through axisymmetric media, *Computer Methods in Applied Mechanics and Engineering* vol.197, pp. 45-48.